Antiferromagnetic ordering in the novel Tm_3Ge_4 compound studied by neutron diffraction and magnetic measurements

1998 J. Phys.: Condens. Matter 10 6553

(http://iopscience.iop.org/0953-8984/10/29/015)

J. Phys.: Condens. Matter **10** (1998) 6553–6564. Printed in the UK PII: S0953-8984(98)91949-X

Antiferromagnetic ordering in the novel Tm_3Ge_4 compound studied by neutron diffraction and magnetic measurements

O Zaharko†¶, P Schobinger-Papamantellos†, W Sikora‡, C Ritter§, Y Janssen‖, E Brück‖, F R de Boer‖ and K H J Buschow‖

† Laboratorium für Kristallographie, ETHZ, CH-8092 Zürich, Switzerland

‡ Faculty of Physics and Nuclear Techniques, Academy of Mining and Metallurgy, Reymonta 19, 30-059 Kraków, Poland

§ Institut Laue–Langevin, 156X, 38042 Grenoble Cédex, France

‖ Van der Waals–Zeeman Institute, University of Amsterdam, 1018 XE Amsterdam, The Netherlands

Received 23 February 1998

Abstract. The magnetic ordering of the novel binary compound Tm_3Ge_4 (Er_3Ge_4 structure type, space group $Cmcm$) has been studied by neutron diffraction, specific heat and magnetic measurements. Antiferromagnetic ordering of Tm_3Ge_4 sets in below $T_N = 2.6$ K and is associated with two wave vectors $\boldsymbol{q}_1 = (0, 1/2, 0)$ and $\boldsymbol{q}_2 = (0, 1, 0)$.

The major magnetic phase with $\boldsymbol{q}_1 = (0, 1/2, 0)$ has a planar canted antiferromagnetic structure. Group theory was used to determine the possible magnetic structures. The two Tm sites (Tm_1 : 8(f) and Tm_2 : 4(c)) order simultaneously with mutually perpendicular orientations. Both sites split into two independent sets under the action of the wave vector $\boldsymbol{q}_1$. The Tm_1 sites have a uniaxial arrangement along the $\boldsymbol{b}$-axis with the same moment values. The Tm_2 sites have a uniaxial moment arrangement along the $\boldsymbol{a}$-axis but two different moment values. At 1.7 K the ordered magnetic moment values are 4.38(5) μ_B/Tm_1, 3.1(2) μ_B/Tm_2 and 0.7(2) μ_B/Tm_2.

The minor magnetic phase with $\boldsymbol{q}_2 = (0, 1, 0)$ has a planar canted antiferromagnetic structure. The Tm_1 and Tm_2 sites order with a uniaxial antiferromagnetic moment arrangement and with mutually perpendicular orientations: along the $\boldsymbol{b}$- and $\boldsymbol{c}$-axis, respectively. At 1.7 K the ordered magnetic moment values are 1.5(1) μ_B/Tm_1 and 0.9(2) μ_B/Tm_2.

1. Introduction

The magnetic ordering in several R_3Ge_4 compounds (R = Tb, Dy, Ho, Er) was recently studied [1–4] by powder neutron diffraction and magnetic measurements. The studied compounds crystallize with the Er_3Ge_4 orthorhombic structure [5] (space group $Cmcm$) which comprises two rare-earth sites, R_1 8(f) and R_2 4(c). The underlying triangular R atom arrangement results in nearest neighbour R–R interactions that lead to magnetic frustration and complex ordering types [4].

The majority of examined R_3Ge_4 compounds (R = Tb, Dy, Ho) displays a two-step magnetic ordering of the two R moments. The moments of the two R sublattices order independently with two distinct order parameters associated with the same wave vector $\boldsymbol{q} = (010)$. The 8(f) site moments order blow T_N; the 4(c) site moments order at lower temperatures.

¶ On leave from the Institute of Inorganic Chemistry, Lviv State University, Lviv, Ukraine.

0953-8984/98/296553+12$19.50

The preferred direction of the magnetic moments changes within the R_3Ge_4 series. The easy axis of antiferromagnetism of the R_1 site moments is defined by the crystal field interaction and lies along the $\boldsymbol{c}$-axis for Ho, along the $\boldsymbol{a}$-axis for Dy and Tb (in the HT region) and in the $(0yz)$ plane for Er. The easy direction of the R_2 site moment tend to be perpendicular to those of the R_1 site and is along the $\boldsymbol{a}$-axis of Ho and along the $\boldsymbol{c}$-axis for Er, Dy and Tb.

We report in this paper on the magnetic structure of Tm_3Ge_4 which differs significantly from that of the previously studied R_3Ge_4 compounds.

2. Sample preparation

Several polycrystalline samples of composition Tm_3Ge_4 were prepared by arc melting of the elements in an atmosphere of purified argon gas. The purity of the starting materials was 99.9% for Tm and 99.99% for Ge. After arc melting the samples were vacuum annealed at 800 °C for three weeks and subsequently quenched in water. The purity of the samples was examined by x-ray powder diffraction. All samples contained several unidentified impurity phases. The single phase condition in this case is encumbered by the high vapour pressure of Tm and by the complexity of the phase diagram around this composition. The best available sample was used for neutron diffraction.

3. Specific heat and magnetic measurements

Magnetic measurements of Tm_3Ge_4 were made with a SQUID magnetometer. The temperature dependence of the reciprocal susceptibility is shown in figure 1. Curie–Weiss behaviour is virtually followed down to the lowest temperature. From the slope and the

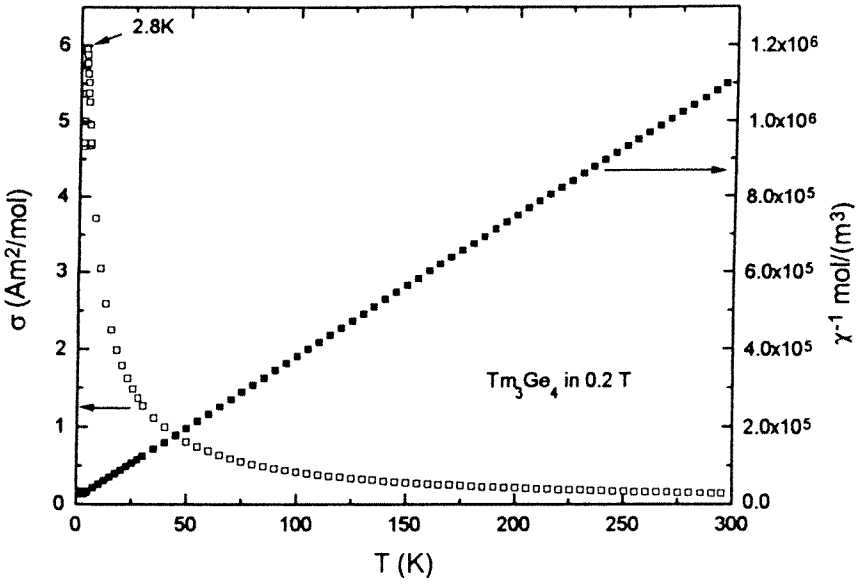

Figure 1. Temperature dependence of magnetization of Tm_3Ge_4 measured in a field of 0.2 T (left scale) and temperature dependence of the reciprocal susceptibility (right scale).

intercept with the horizontal axis we derive the values $\mu_{eff} = 7.63\ \mu_B$/Tm and $\theta_P = -3.8$ K for the effective moment and the asymptotic Curie temperature, respectively. The former value is close to the free ion value (7.57 μ_B/Tm). The temperature dependence of the magnetization, also shown in figure 1, is characterized by an antiferromagnetic type transition at about 2.8 K.

Results of specific heat measurements made on Tm_3Ge_4 are shown in the top left part of figure 2. The low-temperature behaviour is shown in more detail in the top right part of the same figure. There is a broad peak centred around 2.2 K and a shoulder at the high-temperature side of the peak at 2.9 K. The small contribution represented by the shoulder is attributed to the small amounts of an impurity phase, as also found by neutron diffraction described below. The large peak is attributed to magnetic ordering of the main phase.

In order to determine the magnetic contribution to the specific heat of Tm_3Ge_4 we have also performed measurements on the isotypic compound Lu_3Ge_4. Results are shown

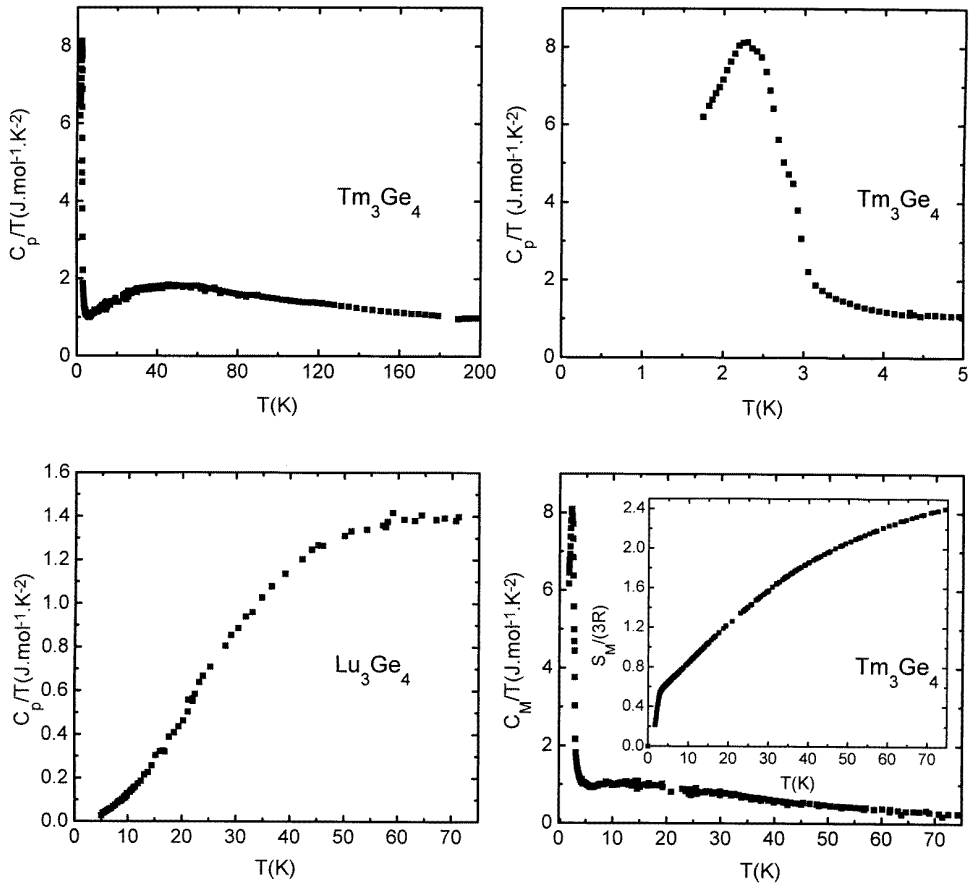

Figure 2. Temperature dependence of the specific heat C_p/T of Tm_3Ge_4 (top left). Low-temperature data in an expanded temperature scale (top right). Temperature dependence of the specific heat C_p/T of Lu_3Ge_4 (bottom left). Magnetic contribution to the specific heat C_p/T of Tm_3Ge_4 (bottom right). The corresponding temperature dependence of the magnetic entropy is shown in the inset. All units are expressed per mol R_3Ge_4.

in the bottom left part of figure 2. Because Lu is nonmagnetic these data can be taken as representative for the lattice contribution of Tm_3Ge_4. These data have been used to determine the lattice contribution and the electronic contribution to the specific heat in Lu_3Ge_4. Subsequently the lattice contribution of Lu_3Ge_4 was corrected for the slightly different atomic mass to obtain the lattice contribution representative for Tm_3Ge_4. The latter contribution together with the electronic contribution was subtracted from the Tm_3Ge_4 data. The corresponding result is representative of the magnetic contribution of Tm_3Ge_4 which is shown in the bottom right part of figure 2. The temperature dependence of the magnetic entropy derived from the magnetic contribution is displayed in the inset. At 75 K the magnetic entropy is seen to be still below the value $S_M/(3R) = \ln(2J + 1) = 2.56$ expected when all $2J + 1$ levels of the ground state manifold were occupied. These results and the comparatively low value of the entropy at T_N are indicative of appreciable crystal field effects. The presence of two crystallographic Tm sites in Tm_3Ge_4 hampers further analysis of the crystal field splitting.

4. Neutron diffraction

Neutron diffraction experiments were carried out at the facilities of the ILL reactor (Grenoble) D1B diffractometer ($\lambda = 2.52$ Å). The data were collected in the temperature range 1.4–50 K, the step increment in 2θ was 0.2°. The data analysis was performed by the Fullprof program [6].

4.1. Crystal structure of Tm_3Ge_4

The neutron patterns in the paramagnetic state confirm the crystal structure of Tm_3Ge_4 as found in [5]. In addition to the main contributions of the Tm_3Ge_4 phase two foreign lines were detected (marked by $\boldsymbol{i}$ in figure 3(a)). These lines do not correspond to phases of the Tm–Ge system reported in [7] therefore they were excluded from the refinement. The results of the 5 K refinement are displayed in figure 3(a) and in table 1.

Table 1. Refined parameters from neutron data of Tm_3Ge_4 (space group $Cmcm$) (a) at 5 K (paramagnetic state), (b) at 1.7 K (magnetically ordered state) of the major magnetic phase ($\boldsymbol{q}_1 = (0, 1/2, 0)$), magnetic space group $P_b12'1$) and the minor magnetic phase ($\boldsymbol{q}_2 = (0, 1, 0)$, magnetic space group $C_p\frac{22'2'_1}{m'cm}i'(\mathrm{Sh}^{391}_{57})$).

	5 K		1.7 K				
			$\boldsymbol{q}_1$			$\boldsymbol{q}_2$	
	y	z	Tm_1	Tm_2^{1o}	Tm_2^{2o}	Tm_1	Tm_2
Tm_1 8f: $(0, y, z)$	0.332(1)	0.101(2)					
Tm_2 4c: $(0, y, 1/4)$	0.055(2)	0.25	μ_x [μ_B]	0.7(2)	3.1(2)		
Ge_1 8f: $(0, y, z)$	0.367(2)	0.892(1)	μ_y [μ_B] 4.38(5)			1.5(1)	
Ge_2 4c: $(0, y, 1/4)$	0.773(2)	0.25	μ_z [μ_B]				0.9(2)
Ge_3 4a: $(0, 0, 0)$	0.0	0.0					
a, b, c [Å]	3.9629(9), 10.437(3), 13.988(4)		3.968(1), 10.543(3), 14.005(7)				
R_n, R_{m1}, R_{m2} (%)	5.2, —, —		—, 13.6, 13.5				
R_{wp}, R_{exp} (%)	10.9, 4.1		17.6, 8.9				

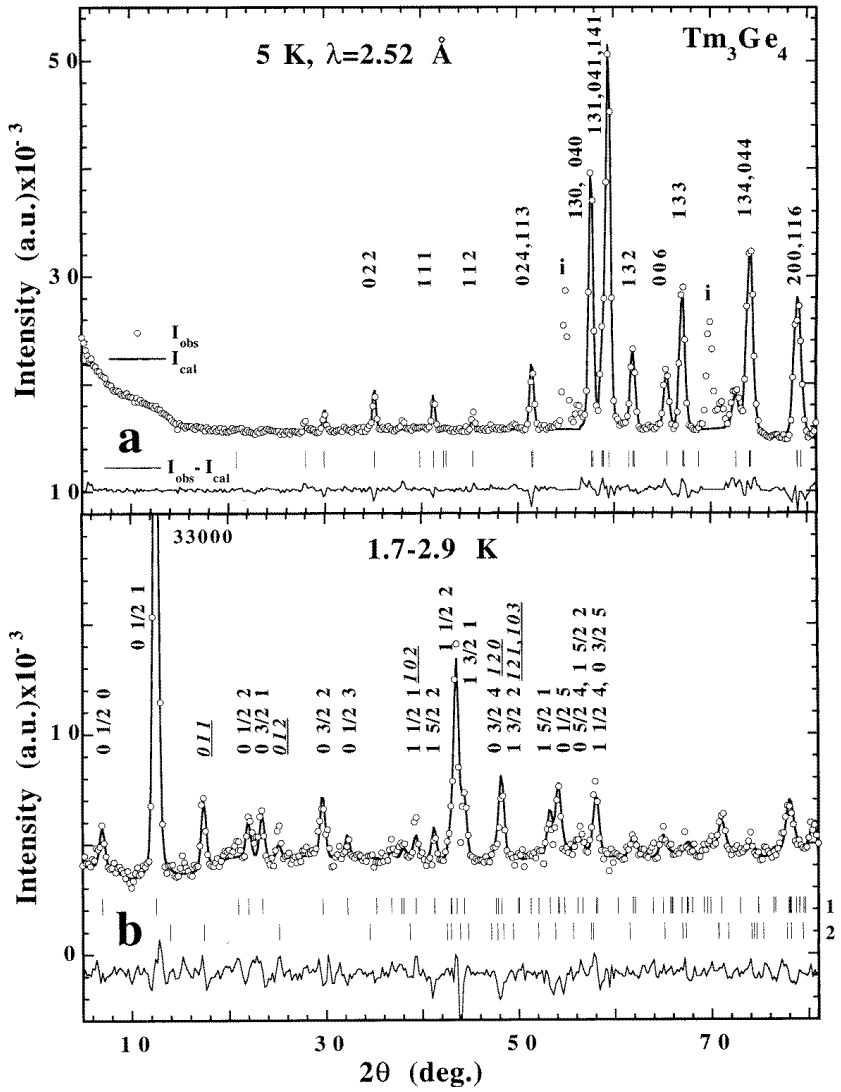

Figure 3. (a) Observed, calculated and difference neutron diagram of Tm_3Ge_4 at 5 K. Unidentified impurity lines (*i*) are supressed in refinement by excluded regions. (b) Observed, calculated and difference neutron diagram (1.7–2.9 K) comprising two sets of magnetic reflections associated with the wave vectors $\boldsymbol{q}_1 = (0, 1/2, 0)$ (indexed in bold) and $\boldsymbol{q}_2 = (0, 1, 0)$ (indexing is underlined). The labels in the margin represent 1—contributions associated with $\boldsymbol{q}_1$, 2—contributions associated with $\boldsymbol{q}_2$.

4.2. Magnetic ordering of Tm_3Ge_4

The 1.7 K neutron pattern comprises next to the nuclear lines magnetic peaks that are not situated at the positions of the nuclear reciprocal lattice of Tm_3Ge_4. The magnetic lines can be classified into three distinct sets.

The dominating *first set* can be indexed using the wave vector $\boldsymbol{q}_1 = (0, 1/2, 0)$ of the orthorhombic nuclear *C*-lattice and leads to the ***b***-anticentred magnetic lattice P_b.

The *second set* comprises only a few weak lines indexed with the wave vector $\boldsymbol{q}_2 = (0, 1, 0)$ associated with an anticentred magnetic C_p-lattice. The topology and the relative intensities of these magnetic reflections are very similar to those observed in Er_3Ge_4 [1].

The *third set* appears at positions not related to the Tm_3Ge_4 lattice and was attributed to the magnetic ordering of the impurity phase which appears below 2.9 K. The intensity of these lines remains constant in the 1.7–2.9 K interval.

The first and the second sets associated with the magnetic ordering of Tm_3Ge_4 evolve in the 1.7–2.4 K temperature interval. In order to overcome the difficulty of calculating coexisting unknown phases we studied the difference diagram obtained by subtracting the 2.9 K data from the 1.7 K data.

The remaining two sets of reflections are exclusively associated with the magnetic ordering of Tm_3Ge_4. In our analysis we considered two cases: (i) two coexisting magnetic structures, (ii) a unique magnetic structure with two propagation vectors. As the magnetic contributions correspond to different Fourier coefficients these two cases cannot be distinguished. The refinement was performed within the assumption of two coexisting magnetic structures.

4.2.1. Magnetic structure ($\boldsymbol{q}_1 = (0, 1/2, 0)$). From the systematic extinctions (hkl with $k = 2n$ absent) observed for the first set of reflections with wave vector $\boldsymbol{q}_1 = (0\,1/2\,0)$ we derived the $\boldsymbol{b}$-anticentred magnetic lattice P_b with the antitranslation $\boldsymbol{t}' = (0\,1\,0)$.

The star of the wave vector has two arms: $\pm\boldsymbol{q}_1 = \pm(0, 1/2, 0)$. The point group of the wave vector g_k comprises four elements: $\{1, m_x, 2_y, m_z\} = C_{2v}$; the corresponding space group G_k is $Cm2m$. The action of the group G_k on the 4(c) and 8(f) positions splits each of

Table 2. Basis vectors of the irreducible representation τ_4 of the $Cmcm$ group with $\{\boldsymbol{q}_1 = (0, 1/2, 0), -\boldsymbol{q}_1\}$ describing ordering of the Tm_1 8(f) site. The coordinates of atoms are: 1—$(0, y, z)$, 2—$(0, y, 1/2 - z)$, 3—$(1/2, 1/2 + y, z)$, 4—$(1/2, 1/2 + y, 1/2 - z)$, 5—$(0, 1 - y, 1 - z)$, 6—$(0, 1 - y, 1 - z)$, 7—$(1/2, 1/2 - y, 1/2 + z)$, 8—$(1/2, 1/2 - y, 1 - z)$ ($y = 0.333, z = 0.101$).

Atoms		1	2	3	4	5	6	7	8
$\boldsymbol{q}_1$	orbit 1	(0 1 0) (0 0 1)	(0 −1 0) (0 0 1)	(0 i 0) (0 0 i)	(0 −i 0) (0 0 i)				
	orbit 2					(0 −1 0) (0 0 1)	(0 1 0) (0 0 1)	(0 i 0) (0 0 −i)	(0 −i 0) (0 0 −i)
$-\boldsymbol{q}_1$	orbit 1					(0 1 0) (0 0 −1)	(0 −1 0) (0 0 −1)	(0 i 0) (0 0 −i)	(0 −i 0) (0 0 −i)
	orbit 2	(0 −1 0) (0 0 −1)	(0 1 0) (0 0 −1)	(0 i 0) (0 0 i)	(0 −i 0) (0 0 i)				

Table 3. Basis vectors of the irreducible representation τ_3 of the $Cmcm$ group with $\{\boldsymbol{q}_1 = (0, 1/2, 0), -\boldsymbol{q}_1\}$ describing ordering of the Tm_2 4(c) site. The coordinates of atoms are: 1—$(0, y, 1/4)$, 2—$(1/2, 1/2 + y, 1/4)$, 3—$(0, 1 - y, 3/4)$, 4—$(1/2, 1/2 - y, 3/4)$, ($y = 0.055$).

Atoms		1	2	3	4
$\boldsymbol{q}_1$	orbit 1	(1 0 0)	(i 0 0)		
	orbit 2			(1 0 0)	(−i 0 0)
$-\boldsymbol{q}_1$	orbit 1			(1 0 0)	(i 0 0)
	orbit 2	(1 0 0)	(−i 0 0)		

them into two inequivalent sets (orbits) (see tables 2 and 3), i.e. for $\boldsymbol{q}_1$ the orbit 1 comprises the atoms 1 and 2 and orbit 2 atoms 3 and 4. The moments of independent orbits may have different values and directions.

The four irreducible representations (IRs) of the *Cmcm* space group for the star $\{\boldsymbol{q}_1 = (0, 1/2, 0), -\boldsymbol{q}_1\}$ are listed in table 4. They are two dimensional and appear in the magnetic representation in the form:

$$\sigma_m^{\{q1\}} = \sigma_m^{\{q1\}}(4c) \oplus \sigma_m^{\{q1\}}(8f) \tag{1}$$

where

$$\sigma_m^{\{q1\}}(4c) = \tau_2 \oplus \tau_3 \oplus \tau_4 \tag{2}$$

$$\sigma_m^{\{q1\}}(8f) = \tau_1 \oplus 2\tau_2 \oplus \tau_3 \oplus 2\tau_4. \tag{3}$$

(a) Tm_1 8(f) *site*. The refinement of the magnetic intensities has shown that the main antiferromagnetic contributions arise due to the ordering of the Tm_1 moments according to the τ_4 representation. The calculated magnetic modes (the components of the basis vectors associated with the IRs) for the two arms $\pm\boldsymbol{q}_1$ for the τ_4 representation are given in table 2. The refinement indicated that the Tm_1 moments order along the y-direction, therefore the z-component was not considered in the symmetry analysis given below.

Group theory analysis [8] allows us to find all models of magnetic structures compatible with the paramagnetic phase symmetry. These models may be given as the linear combination of the basis vectors of the IRs of group G_k, with coefficients $V\,e^{i\varphi}$ and $-V'\,e^{-i\psi}$. The magnetic moment of any atom at distance $\boldsymbol{t} = n_1\boldsymbol{a}_1 + n_2\boldsymbol{a}_2 + n_3\boldsymbol{a}_3$ obtained for the τ_4 representation of the sine wave modulated structure is given in the equations:

$$\boldsymbol{S}_{1+t} = -\boldsymbol{S}_{3+t} = 2V\cos(\varphi + \boldsymbol{q}_1 \cdot \boldsymbol{t})\boldsymbol{e}_y \tag{4}$$

$$\boldsymbol{S}_{2+t} = -\boldsymbol{S}_{4+t} = -2V'\cos(\psi + \boldsymbol{q}_1 \cdot \boldsymbol{t})\boldsymbol{e}_y \tag{5}$$

$$\boldsymbol{S}_{5+t} = -\boldsymbol{S}_{7+t} = -2V\sin(\varphi + \boldsymbol{q}_1 \cdot \boldsymbol{t})\boldsymbol{e}_y \tag{6}$$

$$\boldsymbol{S}_{6+t} = -\boldsymbol{S}_{8+t} = -2V'\sin(\psi + \boldsymbol{q}_1 \cdot \boldsymbol{t})\boldsymbol{e}_y \tag{7}$$

where $2V$ and $2V'$ are the amplitudes of the wave and φ and ψ the phase factors in fractions of 2π. According to Landau's theory of continuous phase transitions [9, 10] the values p_1 and p_2 composed from the mixing coefficients in the way: $p_1 = (V\,e^{i\varphi}; -V'\,e^{-i\psi})$ for the first orbit and $p_2 = (V'\,e^{i\psi}; -V\,e^{-i\varphi})$ for the second orbit of the Tm_1 site have the meaning of order parameters of the phase transition.

As follows from the refinement, the coefficients V and V' have the same value but opposite signs: $V' = -V = 4.38(5)\ \mu_B$, when choosing $\varphi = \psi = \pi/4$. The resulting uniaxial arrangement of the Tm_1 moments is then described by the sequence A_y–A_y $(+\ -\ -\ +\ +\ -\ -+)$ for atoms 1–8 listed in table 2 in the notation of [11] and remains invariant under the transformations of the magnetic space group $P_bm'2'm$. The possible magnetic space group related to a given representation can be found by action of the elements of the *Cmcm* space group on the order parameters (see table 4, last column).

This model, however, could not fully explain all observations. The major discrepancy is the existence of a weak (0 1/2 0) magnetic line at $2\theta = 6.85^\circ$ in the difference 1.7 K–2.9 K neutron diagram. This reflection can only arise from contributions along x or z. The best agreement between observed and calculated data was obtained for the Tm_2 moments aligned along the x-axis.

Table 4. Representative matrices of irreducible representations of the $Cmcm$ group for the star $\{\boldsymbol{q}_1 = (0, 1/2, 0), -\boldsymbol{q}_1\}$ and possible magnetic space groups.

Representation	e	2_x	2_y	2_{1z}	i	m_x	c_y	m_z	Magnetic group
τ_1	$\begin{pmatrix}1&0\\0&1\end{pmatrix}$	$\begin{pmatrix}0&1\\1&0\end{pmatrix}$	$\begin{pmatrix}1&0\\0&1\end{pmatrix}$	$\begin{pmatrix}0&1\\1&0\end{pmatrix}$	$\begin{pmatrix}0&1\\1&0\end{pmatrix}$	$\begin{pmatrix}1&0\\0&1\end{pmatrix}$	$\begin{pmatrix}0&1\\1&0\end{pmatrix}$	$\begin{pmatrix}1&0\\0&1\end{pmatrix}$	P_bm2m
τ_2	$\begin{pmatrix}1&0\\0&1\end{pmatrix}$	$\begin{pmatrix}0&1\\1&0\end{pmatrix}$	$\begin{pmatrix}1&0\\0&1\end{pmatrix}$	$\begin{pmatrix}0&1\\1&0\end{pmatrix}$	$\begin{pmatrix}0&-1\\-1&0\end{pmatrix}$	$\begin{pmatrix}-1&0\\0&-1\end{pmatrix}$	$\begin{pmatrix}0&-1\\-1&0\end{pmatrix}$	$\begin{pmatrix}-1&0\\0&-1\end{pmatrix}$	$P_bm'2m'$
τ_3	$\begin{pmatrix}1&0\\0&1\end{pmatrix}$	$\begin{pmatrix}0&-1\\-1&0\end{pmatrix}$	$\begin{pmatrix}-1&0\\0&-1\end{pmatrix}$	$\begin{pmatrix}0&1\\1&0\end{pmatrix}$	$\begin{pmatrix}0&-1\\-1&0\end{pmatrix}$	$\begin{pmatrix}1&0\\0&1\end{pmatrix}$	$\begin{pmatrix}0&1\\1&0\end{pmatrix}$	$\begin{pmatrix}-1&0\\0&-1\end{pmatrix}$	$P_bm2'm'$
τ_4	$\begin{pmatrix}1&0\\0&1\end{pmatrix}$	$\begin{pmatrix}0&-1\\-1&0\end{pmatrix}$	$\begin{pmatrix}-1&0\\0&-1\end{pmatrix}$	$\begin{pmatrix}0&1\\1&0\end{pmatrix}$	$\begin{pmatrix}0&1\\1&0\end{pmatrix}$	$\begin{pmatrix}-1&0\\0&-1\end{pmatrix}$	$\begin{pmatrix}0&-1\\-1&0\end{pmatrix}$	$\begin{pmatrix}1&0\\0&1\end{pmatrix}$	$P_bm'2'm$

(b) *Tm_2 4(c) site*. The arrangement of the Tm_2 magnetic moments is described by the τ_3 representation. As mentioned above for Tm_1, a linear combination of the IR basis functions (see table 3), with mixing coefficients given as components of the order parameters $p_1 = (U\,e^{i\varphi}; U'\,e^{-i\psi})$ and $p_2 = (U'\,e^{i\psi}; U\,e^{-i\varphi})$ for the first and second orbit, respectively, gives the ordering of the magnetic moments:

$$\boldsymbol{S}_{1+t} = 2U\cos(\varphi + \boldsymbol{q}_1 \cdot \boldsymbol{t})\boldsymbol{e}_x \tag{8}$$

$$\boldsymbol{S}_{2+t} = -2U\sin(\varphi + \boldsymbol{q}_1 \cdot \boldsymbol{t})\boldsymbol{e}_x \tag{9}$$

$$\boldsymbol{S}_{3+t} = 2U'\cos(\psi + \boldsymbol{q}_1 \cdot \boldsymbol{t})\boldsymbol{e}_x \tag{10}$$

$$\boldsymbol{S}_{4+t} = 2U'\sin(\psi + \boldsymbol{q}_1 \cdot \boldsymbol{t})\boldsymbol{e}_x. \tag{11}$$

As follows from the refinement, the coefficients U and U' have different values $2U = 3.1(2)\ \mu_B$ and $2U' = 0.7(2)\ \mu_B$, even when choosing the phase factors $\varphi = \psi = \pi/4$. The resulting uniaxial arrangement of the Tm_2 moments can be described by the sequence A_x $(+-)$ for atoms 1, 2 and F_x $(++)$ for atoms 3,4 listed in table 3 and remains invariant under the transformations of the magnetic space group $P_bm2'm'$.

The ordering of the two Tm sites is described by different magnetic space groups: $P_bm'2'm$ for Tm_1 and $P_bm2'm'$ for Tm_2. The resulting magnetic space group, being the intersection of the two individual groups has only monoclinic symmetry $P_b12'1$.

The total planar canted antiferromagnetic structure (figure 4) splits into four orbits: two Tm_1 orbits and two Tm_2 orbits. The Tm_1 orbits have the same moment value and the same

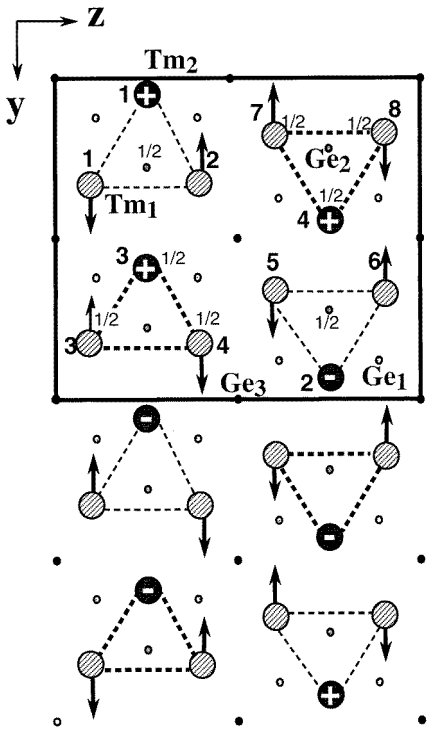

Figure 4. The projection of the magnetic structure of Tm_3Ge_4 ($\boldsymbol{q}_1 = (0, 1/2, 0)$) along the x-axis. $+$ and $-$ denote the Tm_2 μ_x moment component along x. The atom numbers refer to those of tables 2 (Tm_1) and 3 (Tm_2).

direction. The moments of two Tm_2 orbits have the same direction but different moment values. Both sites have a uniaxial antiferromagnetic moment arrangement but with mutually perpendicular orientations. The 1.7 K ordered moment values are $\mu_{1y} = 4.38(5)\ \mu_B$ for the Tm_1 site, $\mu_{2z} = 3.1(2)\ \mu_B$ and $\mu_{2z} = 0.7(2)\ \mu_B$ for the Tm_2 site. These values are considerably lower than the free-ion value of Tm^{3+} ($gJ\ [\mu_B] = 7\ [\mu_B]$) presumably due to crystal field effects and the magnetic frustration due to the triangular arrangement.

4.2.2. Magnetic structure ($\boldsymbol{q}_2 = (0, 1, 0)$). The main magnetic (011, 012) lines arising at positions of the anticentred magnetic C_p-lattice with $\boldsymbol{q}_2 = (0, 1, 0)$ have the same relative intensities as observed in Er_3Ge_4 [1]. Therefore the model of the Er_3Ge_4 magnetic structure was implemented. The two Tm sites order with a uniaxial collinear antiferromagnetic arrangement in two mutually perpendicular directions. The Tm_1 magnetic moments order along y, the Tm_2 moments along the z-axis. The z-component of the R_1 moments observed for Er_3Ge_4 is negligible for Tm_3Ge_4. The 1.7 K ordered moment values are $\mu_{1y} = 1.5(1)\ \mu_B$ for the Tm_1 site and $\mu_{2z} = 0.9(2)\ \mu_B$ for the Tm_2 site. These values are considerably lower than the free-ion value of Tm^{3+} and indicate that the amount of this magnetic phase in the studied sample is small.

The rather high values of the reliability factors $R_{m1} = 13.6\%$, $R_{m2} = 13.5\%$, $R_{wp} = 17.6\%$ between experimental and calculated patterns result from the low counting statistics of the difference diagram. Furthermore the difference diagram (1.7–2.9 K) assumes no changes of the magnetic structure of the impurity phase at 1.7 K which cannot be excluded from the present data.

4.3. Thermal evolution of magnetic intensities in Tm_3Ge_4

The thermal variation of some selected magnetic integrated intensities of Tm_3Ge_4 is shown in figure 5. The (0 1/2 1) and (0 1/2 0) lines correspond to the wave vector $\boldsymbol{q}_1 = (0, 1/2, 0)$; the (011) line is associated with the wave vector $\boldsymbol{q}_2 = (0, 1, 0)$. It can be seen that the ordering temperature is the same for all magnetic contributions of Tm_3Ge_4 and is equal to

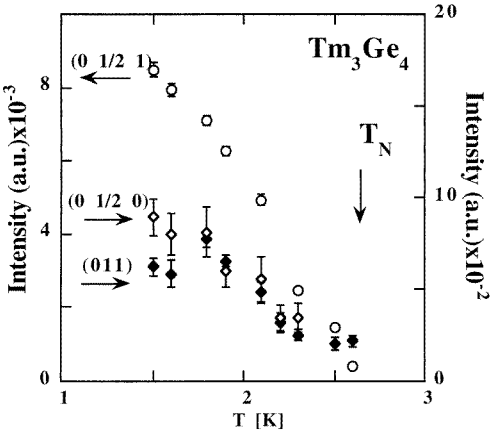

Figure 5. Temperature dependence of the magnetic intensity of the (0 1/2 1), (0 1/2 0) lines associated with the wave vector $\boldsymbol{q}_1 = (0,\ 1/2,\ 0)$ and of the (011) line associated with the wave vector $\boldsymbol{q}_2 = (0,\ 1,\ 0)$ of Tm_3Ge_4.

$T_N = 2.6$ K. The magnetic (0 1/2 1) line at $2\theta = 12.5^\circ$ is dominant in the whole 1.7–2.7 K temperature interval, this can be explained by the dominant μ_{1y} contribution of the Tm_1 moment into the magnetic structure factor of the (0 1/2 1) line:

$$F(0\,1/2\,1) \sim 2 \times 1.40\boldsymbol{\mu}_{1y} + 0.6\boldsymbol{\mu}_{2x}^{1o} - 1.28\mu_{2x}^{2o} \tag{12}$$

(the superscripts $1o$ and $2o$ stand for the first and second orbit, respectively).

The magnetic (0 1/2 0) line at $2\theta = 6.9^\circ$ has only a magnetic μ_{2x} contribution of the Tm_2 first orbit:

$$F(0\,1/2\,0) \sim 1.28\boldsymbol{\mu}_{2x}^{1o}. \tag{13}$$

The monotonic thermal evolution of the (0 1/2 1) and (0 1/2 0) lines implies that the Tm_1 and Tm_2 magnetic moments order at the same temperature.

5. Conclusions

The magnetic ordering of the novel phase Tm_3Ge_4 was studied by neutron diffraction, magnetic measurements and specific heat measurements. The Tm_3Ge_4 compound exhibits a type of magnetic ordering different from that observed in other R_3Ge_4 compounds (R = Tb, Dy, Ho, Er).

A characteristic feature of the Tm_3Ge_4 magnetic structure is the presence of the antitranslation along $\boldsymbol{b}$, which leads to the sign inversion of the magnetic moments in adjacent crystallographic unit cells along this direction.

The triangular arrangement of the Tm sites within the $(0yz)$ plane with AF interaction causes a geometrical frustration of the magnetic moments. Although the two Tm sublattices order simultaneously, the moments of the two Tm sites have mutually perpendicular directions. The common trend of the easy moment direction for the R_2 site to be perpendicular to those of the R_1 site as described extensively in [4] is preserved in Tm_3Ge_4. In the resulting planar canted antiferromagnetic arrangement the Tm_1 moments are aligned along the y-axis, similarly to Er_3Ge_4, with the dominant y-component. The Tm_2 moments lie along the x-axis similarly to Ho_3Ge_4.

The coexistence of two magnetic structures with two different wave vectors $\boldsymbol{q}_1 = (0, 1/2, 0)$ and $\boldsymbol{q}_2 = (0, 1, 0)$ indicates that the free energy space has two minima, which are close in value in a very narrow temperature range. Here it should be noted that there is ambiguity in the derived moment values of the two magnetic phases as they refer to one and the same crystallographic phase and their relative amounts cannot be extracted by powder diffraction. The magnetic ordering with two different wave vectors and the concomitant different temperature dependences is also reflected in the relative broadness of the specific heat peak associated with the overall antiferromagnetic ordering.

Acknowledgments

This work is financially supported by the Swiss National Foundation and by the Polish State Committee for Scientific Research.

References

[1] Schobinger-Papamantellos P, Oleksyn O, Ritter C, de Groot C H and Buschow K H J 1997 *J. Magn. Magn. Mater.* **169** 253

[2] Oleksyn O, Schobinger-Papamantellos P, Ritter C, de Groot C H and Buschow K H J 1997 *J. Alloys Compounds* **262/263** 492
[3] Oleksyn O, Schobinger-Papamantellos P, Ritter C, Janssen Y, Brück E and Buschow K H J 1997 *J. Phys.: Condens. Matter* **9** 1
[4] Zaharko O, Schobinger-Papamantellos P, Ritter C, Janssen Y, Brück E and Buschow K H J 1997 *J. Phys.: Condens. Matter* **10** 2881
[5] Oleksyn O Ya and Bodak O I 1994 *J. Alloys Compounds* **210** 19
[6] Rodríguez-Carvajal J 1993 *Physica* B **192** 55
[7] Eremenko V N, Meleshevich K A, Buyanov Yu I and Martsenyuk P S 1989 Translated from *Poroshkovaya Metallurgiya* **7** 41
[8] Izyumov Yu A, Naish V E and Ozerov R P 1991 *Neutron Diffraction of Magnetic Materials* (New York: Consultants Bureau)
[9] Landau L D and Lifshits E M 1959 *Statistical Physics* (Oxford: Pergamon)
[10] Izyumov Yu A and Syromyatnikov V N 1990 *Phase Transitions and Crystal Symmetry* (Dordrecht: Kluwer)
[11] Bertaut E F 1975 *Ann. Phys., Paris* **9** 93
Bertaut E F 1968 *Acta Crystallogr.* A **24** 217
Bertaut E F 1963 *Magnetism* vol 3, ed G T Rado and H Suhl (New York: Academic) ch 4, p 149